Journal of Quantitative Spectroscopy & Radiative Transfer 152 (2015) 28–36

Contents lists available at ScienceDirect

Journal of Quantitative Spectroscopy & Radiative Transfer

journal homepage: www.elsevier.com/locate/jqsrt

A theoretical room-temperature line list for $^{15}NH_3$

Sergei N. Yurchenko*

Department of Physics and Astronomy, University College London, London WC1E 6BT, UK

ARTICLE INFO

Article history:
Received 30 June 2014
Received in revised form
27 October 2014
Accepted 30 October 2014
Available online 7 November 2014

Keywords:
Ammonia
IR
Linelist
ab initio
HITRAN
Absorption

ABSTRACT

A new room temperature line list for $^{15}NH_3$ is presented. This line list comprised of transition frequencies and Einstein coefficients has been generated using the 'spectroscopic' potential energy surface NH3-Y2010 and an *ab initio* dipole moment surface. The $^{15}NH_3$ line list is based on the same computational procedure used for the line list for $^{14}NH_3$ BYTe reported recently and should be as accurate. Comparisons with experimental frequencies and intensities are presented. The synthetic spectra show excellent agreement with experimental spectra.

1. Introduction

Although the abundance of ^{15}N is 450 times lower than that of ^{14}N [1], $^{15}NH_3$ is an important astrophysical molecule. It is a maser source detected in interstellar molecular clouds [2] and is also a tracer of the $^{15}N/^{14}N$ isotopic ratio in interstellar medium [3–5], planetary [6,7] and Earth [8] atmospheres, meteorites [9], comets [10], important as a probe of chemical processes in the astrophysical environment, of planetary atmospheric and formation processes etc. Very recently Fletcher et al. [11] used the $^{14}NH_3$ and $^{15}NH_3$ spectral features to study the $^{15}N/^{14}N$ ratio for Jupiter and Saturn.

Experimentally the ro-vibrational spectra of $^{15}NH_3$ have been studied in a large number of works, including rotation-inversion spectra [12–17], fundamental bands [18–27], overtone bands [28–33], hot bands [34–37], and intensity measurements [38–41]. Some of these data are now collected in the HITRAN database [42]. The electric dipole moment was experimentally studied by Orr and Oka [43] and Dilonardo et al. [44] using the Stark spectroscopy. The ground state energies were reported by Urban et al. [22]. Very recently a VECSEL laser source study of the 2.3 μm region of $^{15}NH_3$ was presented by Čermák et al. [45] and a tentative assignment of new $^{15}NH_3$ lines in the 1.51 μm region was suggested by Földes et al. [46].

Huang et al. [47] presented theoretical ro-vibrational energies of $^{15}NH_3$ computed variationally using an empirical PES HSL-2 for $J = 0\ldots 6$. These energies helped them to reassign and correct a number of transitions in HITRAN. An extensive hot line list BYTe for $^{14}NH_3$ was recently generated [48] using the TROVE approach [49]. Containing 1.1 billion transitions BYTe was designed to be applicable for temperatures up to 1500 K. It has proven to be useful for astrophysical and spectroscopic applications (see, for example, Refs. [45,50,51]). In this work we build a room temperature line list for the ^{15}N isotopologue of ammonia using the same computational approach based on the 'spectroscopic' potential energy surface (PES) NH3-Y2010 [52] and the *ab initio* dipole moment surface (DMS) from Ref. [53]. The highest J considered in this work is 18 defining the temperature limit of the current line list to be 300 K. It should be noted that TROVE was also used in

* Tel.: +44 2076790172; fax: +44 2076797145.
E-mail address: s.yurchenko@ucl.ac.uk

http://dx.doi.org/10.1016/j.jqsrt.2014.10.023
0022-4073/

Table 1
Comparison of the theoretical term values (cm^{-1}) of $^{15}NH_3$ before EBSC replacement and experimental ones used in the EBSC approach. See Table 7 for the description of the notations.

Γ_{vib}	v_1	v_2	v_3	v_4	L_3	L_4	L_4	Obs.	Calc.	Obs.-Calc.	Ref.
A_2''	0	0	0	0	0	0	0	0.761	0.758	0.003	[35]
A_1'	0	1	0	0	0	0	0	928.509	928.457	0.052	[35]
A_2''	0	1	0	0	0	0	0	962.912	962.894	0.018	[35]
A_1'	0	2	0	0	0	0	0	1591.236	1591.185	0.051	[28][a]
E'	0	0	0	0	1	1	1	1623.130	1623.149	−0.020	[28][b]
E''	0	0	0	0	1	1	1	1624.190	1624.202	−0.012	[28][b]
A_2''	0	2	0	0	0	0	0	1870.823	1870.853	−0.030	[30]
A_1'	0	3	0	0	0	0	0	2369.274	2369.314	−0.041	[28]
E'	0	1	0	0	1	1	1	2533.382	2533.380	0.002	[28][b]
E''	0	1	0	0	1	1	1	2577.571	2577.590	−0.020	[28][b]
A_2''	0	3	0	0	0	0	0	2876.144	2876.130	0.014	[28][a]
A_1'	0	0	0	0	2	0	0	3210.614	3210.430	0.184	[27]
A_2''	0	0	0	0	2	0	0	3212.335	3212.120	0.215	[27]
E'	0	0	0	0	2	2	2	3234.107	3233.925	0.182	[27]
E''	0	0	0	0	2	2	2	3235.504	3235.338	0.165	[27]
A_1'	1	0	0	0	0	0	0	3333.306	3333.220	0.086	[27]
A_2''	1	0	0	0	0	0	0	3334.252	3334.160	0.092	[27]
E'	0	0	1	1	0	0	1	3435.167	3435.143	0.024	[27]
E''	0	0	1	1	0	0	1	3435.540	3435.475	0.065	[27]
A_1'	1	1	0	0	0	0	0	4288.186	4288.024	0.162	[22]
A_2''	1	1	0	0	0	0	0	4312.345	4312.304	0.041	[22]
E'	1	0	0	0	2	2	2	6546.951	6546.987	−0.036	[60]
E''	1	0	0	0	2	2	2	6548.560	6548.449	0.111	[60]
E'	1	0	1	1	0	0	1	6596.569	6596.605	−0.036	[32]
E''	1	0	1	1	0	0	1	6597.607	6597.498	0.109	[32]
E'	1	0	1	1	0	0	1	6664.486	6664.627	−0.141	[33]
E''	1	0	1	1	0	0	1	6665.480	6665.303	0.177	[33]

[a] Estimated from the $a \rightarrow s$ band centers.
[b] Estimated from the corresponding $^{P}P(J=1, k=1)$ transition frequencies.

the study of the thermal averaging properties of the spin–spin coupling constants of $^{15}NH_3$ by Yachmenev et al. [54] and a high-temperature partition function for $^{14}NH_3$ [55].

The paper is structured as follows. In Section 2 we outline the theoretical approach used for the line list production. In Section 3 the structure of the line list and the description of the quantum numbers are presented, where some comparisons with experimental data are also given and the accuracy of the line list is discussed.

2. Theoretical approach

We use the same computational procedure and the associated program TROVE [49] as was employed to generate the hot ammonia line list BYTe [48], therefore the reader should refer to this paper for a detailed description. Here we present only a short outline of this approach.

In order to obtain energies and associated wavefunctions required for building the line list of $^{15}NH_3$ we solve the Schrödinger equation for the nuclear motion variationally. Both the kinetic and potential energy terms of the Hamiltonian were expanded to 6th and 8th orders, respectively, in terms of five linearized coordinates around the reference geometry, defined as a non-rigid reference configuration associated with the inversion motion characterized by a relatively low barrier to the planarity. The linearized coordinates are chosen to be close to the three stretching modes associated with the N–H vibrations and two asymmetric bending modes combined from the three bending vibrations of the interbond angles H–N–H. Our vibrational basis set is a product of six one-dimensional (1D) basis functions. The stretching, bending, and inversion 1D basis sets are obtained by solving the corresponding reduced 1D Schrödinger equations using the Numerov–Cooley approach [56,57] for each degree of freedom independently. This so-called primitive basis set is then improved through a number of pre-diagonalizations and consecutive contractions. The latter is controlled by the polyad number:

$$P = 2(v_1 + v_2 + v_3) + v_4 + v_5 + v_6/2, \quad (1)$$

where v_1, v_2, v_3 are the quantum numbers associated with the three stretching modes, v_4, v_5 are associated with the asymmetric bending modes, and v_6 counts the inversion mode functions. As in Ref. [48], we define the size of the basis set using the condition $P \leq 14$. We use the so-called $J=0$ representation, where the final contracted ro-vibrational basis functions are represented by direct symmetrized products of the vibrational $J=0$ eigenfunctions and the rigid rotor wavefunctions $|J, K, \tau_{rot}\rangle$, where J is the rotational angular momentum, K is the projection of the

rotational angular momentum to the molecular axis z, and $\tau_{\rm rot}$ is the rotational parity (see [58] for further details). The $J=0$ eigenfunctions are the eigensolutions of the pure vibrational problem. The highest rotational excitation presently considered is $J=18$. We only compute and store the energy term values and wavefunctions below 14 000 cm^{-1} above the zero point energy (ZPE) obtained as 7414.08 cm^{-1}. These thresholds are chosen to get a reasonable population at room temperature according with the Boltzmann distribution.

As in [53] here we employ the EBSC (empirical basis set correction) scheme, where some of the $J=0$ band centers are substituted with the corresponding experimental values, where available. For $^{15}NH_3$ however there are only very few band centers known experimentally with high enough accuracy, namely for ν_1, ν_2, ν_3, ν_4, $\nu_1+\nu_2$, $\nu_1+\nu_3$, $2\nu_2$, $\nu_2+\nu_3$, $2\nu_4^{l=0}$, $2\nu_4^{l=2}$, $\nu_1+2\nu_4$, $\nu_2+2\nu_4$, $2\nu_2+\nu_3$, $\nu_3+2\nu_4$ as well as the ground state inversion splitting [18–23,25,27–30,32,33,35–37,45,59,60]. Therefore the effect of this otherwise very efficient procedure is rather limited. With this approach the $J=0$ energies are reproduced exactly, while the ro-vibrational coupling leads to a gradual 'de-focus' of the $J>0$ energies. In Table 1 we compare the original theoretical term values with the experimental band centres used in our EBSC approach. The Obs.-Calc. residuals in this table illustrate the deficiency of our model based on the $^{14}NH_3$ PES applied for the 15th isotopologue. Although the accuracy of these particular bands is recovered through the EBSC approach, the error of other band centers can be expected to be as large as up to about 0.2 cm^{-1} at least, as illustrated in Table 1.

The same PES and DMS as in [48] were used. The potential energy surface NH3-Y2010 was obtained by Yurchenko et al. [52] by fitting to the experimentally derived term values of the main isotopologues only, with $J\leq 8$ covering term values up to $E=10\,300$ cm^{-1}. Because of the approximations used in the fitting, this 'spectroscopic' PES is an effective object. Therefore it does not guarantee, at least in principle, the same accuracy for $^{15}NH_3$ as was reached for $^{14}NH_3$. We make a comparison with the experiment in the next section. The *ab initio* dipole moment surface ATZfc DMS used here was developed by Yurchenko et al. [61] which should be capable of accurate modelling of $^{15}NH_3$ spectra. For the description of the intensity calculations see Refs. [48,62].

In Tables 2–5 we compare our theoretical term values of $^{15}NH_3$ with their 'experimental' counterparts for the vibrational ($J=0$) and pure rotational ($J=0\ldots4$) states available in the literature (see Introduction). As far as the accuracy of these term values is concerned it is comparable to the accuracy of the vibrational term values for the main isotopologue using the same PES. The pure rotational and rotation-inversional term values also show a very good agreement with experiment. This is reassuring especially if the underlying PES was generated using the main isotopologue only, although the effect from the isotopic substitution 14→15 is not expected to be large.

In Table 6 some vibrational term values ($J=0$) of $^{15}NH_3$ from this work are compared to the theoretical values computed by Huang et al. [47] using their empirical PES HSL-II. The agreement at lower energies is very good but deteriorates at about 5000 cm^{-1}. It is difficult to claim the better accuracy for any of these two approaches based on this comparison only. We believe that at least some of our band centers above 6000 cm^{-1} should be more accurate, see e.g. Table 5. However according to Čermák et al. [45] the line positions of $^{15}NH_3$ reported by Huang et al. [47] are more precise at least for the 2.3 μm region.

We have compared our intensities to the HITRAN data [42] as well as to those reported by Devi et al. [39] (ν_4) and Lins et al. [41] (near infrared). In Figs. 1 and 2 we show a generated absorption spectrum of $^{15}NH_3$ at $T=296$ K compared to the HITRAN intensities. The agreement is similar to that achieved by BYTe for $^{14}NH_3$ [48]. The $^{15}NH_3$ experimental data is rather sparse compared to the data available for the main isotopologue. A number of obvious outliers (5014.4776, 5084.8734, 5104.2963, and possibly 5103.8909 cm^{-1}) in the experimental spectra indicate problems with the assignment of the $^{15}NH_3$ transitions in HITRAN. Similar problems have recently been studied and resolved for the $^{14}NH_3$ data [63]. Another outlier is at 6586.747 cm^{-1} from the recent work by Lins et al. [41] which also appears to be too strong, see Figs. 1 and 2.

Table 2
Calculated term values (cm^{-1}) of $^{15}NH_3$ compared to the experimental values [22]: ground vibrational state. Here J is the rotational angular momentum, K is its projection, $\Gamma_{\rm tot}$ is the symmetry of the rotational states $D_{3\,h}$(M), and s/a is the inversion parity.

J	K	$\Gamma_{\rm tot}$	s/a	Obs.	Calc.	Obs.-Calc.
0	0	A_2''	a	0.7577	0.7577	0.0000
1	1	E''	s	16.1491	16.1495	−0.0004
1	1	E'	a	16.9038	16.9042	−0.0004
1	0	A_2'	s	19.8413	19.8416	−0.0003
1	0	A_1''	a	20.5892	20.5895	−0.0003
2	2	E'	s	44.7490	44.7502	−0.0011
2	2	E''	a	45.5046	45.5058	−0.0012
2	1	E''	s	55.8176	55.8186	−0.0010
2	1	E'	a	56.5529	56.5540	−0.0011
2	0	A_1'	s	59.5035	59.5044	−0.0009
2	0	A_2''	a	60.2322	60.2332	−0.0010
3	3	A_1''	s	85.7924	85.7948	−0.0024
3	3	A_2''	s	85.7924	85.7948	−0.0024
3	3	A_2'	a	86.5526	86.5550	−0.0025
3	2	E'	s	104.2293	104.2314	−0.0021
3	2	E''	a	104.9559	104.9582	−0.0022
3	1	E''	s	115.2695	115.2715	−0.0019
3	1	E'	a	115.9768	115.9789	−0.0021
3	0	A_2'	s	118.9460	118.9479	−0.0019
3	0	A_1''	a	119.6469	119.6490	−0.0021
4	4	E'	s	139.2674	139.2715	−0.0041
4	4	E''	a	140.0361	140.0403	−0.0042
4	3	A_2''	s	165.0675	165.0711	−0.0037
4	3	A_2'	a	165.7832	165.7931	−0.0099
4	2	E'	s	183.4416	183.4450	−0.0035
4	2	E''	a	184.1315	184.1352	−0.0038
4	1	E''	s	194.4443	194.4477	−0.0034
4	1	E'	a	195.1158	195.1196	−0.0037
4	0	A_1'	s	198.1083	198.1117	−0.0034
4	0	A_2''	a	198.7738	198.7775	−0.0037

Table 3
Calculated term values (cm^{-1}) of $^{15}NH_3$ compared to the experimental values [22]: ν_2 state. Here J is the rotational angular momentum, K is its projection, Γ_{tot} is the total symmetry of the ro-vibrational states D_{3h}(M), and s/a is the inversion parity.

J	K	Γ_{tot}	State	s/a	Obs.	Calc.	Obs.-Calc.
0	0	A_1'	ν_2	s	928.457	928.457	0.000
1	1	E''	ν_2	s	944.594	944.590	0.004
1	0	A_2'	ν_2	s	948.550	948.544	0.006
0	0	A_2''	ν_2	a	962.894	962.894	0.000
2	2	E'	ν_2	s	972.908	972.898	0.010
1	1	E'	ν_2	a	978.924	978.922	0.003
2	1	E''	ν_2	s	984.763	984.749	0.015
2	2	E''	ν_2	a	1007.269	1007.262	0.007
3	3	A_2''	ν_2	s	1013.390	1013.371	0.019
2	1	E'	ν_2	a	1018.391	1018.382	0.009
2	0	A_2''	ν_2	a	1022.096	1022.086	0.010
3	2	E'	ν_2	s	1033.137	1033.111	0.027
3	1	E''	ν_2	s	1044.949	1044.918	0.031
3	3	A_2'	ν_2	a	1047.921	1047.908	0.013
3	0	A_2'	ν_2	s	1048.881	1048.848	0.032
4	4	E'	ν_2	s	1066.029	1065.998	0.030
3	2	E''	ν_2	a	1066.450	1066.433	0.017
3	1	E'	ν_2	a	1077.544	1077.531	0.013
4	3	A_2''	ν_2	s	1093.666	1093.626	0.040
4	4	E''	ν_2	a	1100.870	1100.848	0.022
4	2	E'	ν_2	s	1113.317	1113.270	0.047
4	1	E''	ν_2	s	1125.071	1125.020	0.051
4	3	A_2'	ν_2	a	1126.801	1126.774	0.026
4	2	E''	ν_2	a	1145.279	1145.249	0.030
4	1	E'	ν_2	a	1156.349	1156.317	0.032
4	0	A_2''	ν_2	a	1160.036	1160.003	0.032

3. The line list

Our room temperature $^{15}NH_3$ line list contains 80 515 767 transitions representing all non-zero (T= 300 K) intensities covering the wavenumber range up to 8000 cm^{-1} constructed from 270 646 upper state term values below 14 000 cm^{-1} and 9772 lower state term values below 6000 cm^{-1} with rotational excitations up to J=18. Following Refs. [48,64] we use the two-files ExoMol format [65] to organize the line list for $^{15}NH_3$. The Energy file (see an extract in Table 7) contains the energy term values $\tilde{E}_i$ (cm^{-1}), quantum numbers both in the local and normal mode representations. Each energy record is indexed with a running number i. These indexes are then used in the Transition file (see extract in Table 8) to refer to a pair of states i' and i'' participating in the transition $i''\rightarrow i'$. Apart from these indexes, only the Einstein coefficient $A(i',i'')$ is needed to complete the transition record. With this format the size of the line list is significantly reduced. The line list can be also found via www.exomol.com as a part of the ExoMol project [66]. We also supply a sample Fortran code to be used together with our line list to simulate intensities or cross sections [67]. In fact the unified ExoMol-format of the present $^{15}NH_3$ line list makes this code useful with any line lists stored in this format.

The largest expansion coefficients of the ro-vibrational eigenfunctions were used to assign the corresponding final eigenvalues with the vibrational quantum numbers v_1, v_2, v_3, v_4, v_5, v_6, the rotational quantum numbers J and K, the total symmetry Γ_{tot} as well as the symmetry of the J=0 vibrational basis function Γ_{vib}. Here Γ_{tot} and Γ_{vib} are represented by six irreducible representations A_1', A_2', E', A_1'', A_2'', E'' in the molecular symmetry group D_{3h}(M) [68].

Table 4
Calculated term values (cm^{-1}) of $^{15}NH_3$ compared to the experimental values [22]: The $\nu_1+\nu_2$ band. Here J is the rotational angular momentum, K is its projection, Γ_{tot} is the total symmetry of the ro-vibrational states D_{3h}(M), and s/a is the inversion parity.

J	K	Γ_{tot}	s/a	Obs.	Calc.	Obs.-Calc.
0	1	A_2''	a	4312.303	4312.304	−0.001
1	1	E''	a	4328.148	4328.151	−0.003
2	1	A_2''	a	4370.642	4370.654	−0.012
2	1	E'	a	4367.042	4367.050	−0.008
2	1	E''	a	4356.231	4356.232	−0.001
3	1	E'	a	4425.344	4425.364	−0.020
3	1	E''	a	4414.552	4414.563	−0.011
3	1	A_2'	a	4396.541	4396.539	0.001
1	1	A_2'	s	4307.725	4307.720	0.006
1	1	E''	s	4303.949	4303.944	0.005
2	1	E''	s	4343.333	4343.320	0.013
2	1	E'	s	4332.010	4332.002	0.008
3	1	A_2'	s	4406.116	4406.086	0.029
3	1	E''	s	4402.357	4402.330	0.028
3	1	E'	s	4391.069	4391.046	0.024
3	1	A_2''	s	4372.198	4372.192	0.006
1	1	E'	a	4328.149	4328.151	−0.002
2	1	E'	a	4367.042	4367.050	−0.009
2	1	E''	a	4356.230	4356.232	−0.002
3	1	E'	a	4425.347	4425.364	−0.016
3	1	E''	a	4414.552	4414.563	−0.011
3	1	A_2'	a	4396.543	4396.539	0.003
4	1	E'	a	4503.017	4503.050	−0.033
4	1	E''	a	4492.247	4492.272	−0.025
4	1	A_2'	a	4474.275	4474.288	−0.013
4	1	E''	a	4449.066	4449.061	0.005
1	1	E''	s	4303.949	4303.944	0.005
2	1	E''	s	4343.336	4343.320	0.015
2	1	E'	s	4332.010	4332.002	0.007
3	1	E''	s	4402.358	4402.330	0.029
3	1	E'	s	4391.074	4391.046	0.028
3	1	A_2''	s	4372.207	4372.192	0.015
4	1	E''	s	4480.955	4480.908	0.047
4	1	E'	s	4469.708	4469.668	0.040
4	1	A_2''	s	4450.918	4450.890	0.028
3	1	E'	a	4424.519	4425.364	−0.845
2	1	A_2''	a	4370.642	4370.654	−0.012
2	1	E'	a	4367.042	4367.050	−0.008
3	1	E'	a	4425.346	4425.364	−0.018
3	1	E''	a	4414.552	4414.563	−0.011
0	0	A_2''	a	4506.607	4506.966	−0.359
4	1	E'	a	4503.020	4503.050	−0.030
4	1	E''	a	4492.248	4492.272	−0.024
4	1	A_2'	a	4474.268	4474.288	−0.020
1	1	A_2'	s	4307.724	4307.720	0.005
2	1	E''	s	4343.335	4343.320	0.015
3	1	A_2'	s	4406.115	4406.086	0.029
3	1	E''	s	4402.358	4402.330	0.028
3	1	E'	s	4391.068	4391.046	0.023
4	1	E''	s	4480.955	4480.908	0.048
4	1	E'	s	4469.711	4469.668	0.043
4	1	A_2''	s	4450.924	4450.890	0.033

Table 5
Calculated term values (cm^{-1}) of $^{15}NH_3$ compared to the experimental values [32,33,60]: the 1.5 μm band. Here J is the rotational angular momentum, K is its projection, Γ_{tot} is the total symmetry of the rovibrational states D_{3h}(M), and s/a is the inversion parity.

J	K	Γ_{tot}	State	s/a	Obs.	Calc.	Obs.-Calc.
0	0	E'	$\nu_1+\nu_3$	s	6596.605	6596.569	0.036
0	0	E''	$\nu_1+\nu_3$	a	6597.498	6597.607	−0.109
0	0	E'	$\nu_1+\nu_3$	s	6664.627	6664.627	0.000
0	0	E''	$\nu_1+\nu_3$	a	6665.303	6665.303	0.000
1	1	E''	$\nu_1+\nu_3$	a	6612.935	6612.745	0.190
1	1	E''	$\nu_1+\nu_3$	s	6613.111	6613.311	−0.200
1	1	E'	$\nu_1+\nu_3$	a	6613.987	6614.222	−0.235
1	0	E'	$\nu_1+\nu_3$	s	6616.563	6616.585	−0.022
1	0	E''	$\nu_1+\nu_3$	a	6617.389	6617.375	0.014
1	1	E''	$\nu_1+\nu_3$	s	6680.448	6680.395	0.053
1	1	E'	$\nu_1+\nu_3$	a	6681.159	6680.969	0.190
1	0	E'	$\nu_1+\nu_3$	s	6684.445	6684.459	−0.014
1	0	E''	$\nu_1+\nu_3$	a	6685.051	6685.062	−0.011
2	2	E''	$\nu_1+\nu_3$	a	6641.024	6640.637	0.387
2	2	A_2'	$\nu_1+\nu_3$	s	6642.655	6642.223	0.432
2	1	E''	$\nu_1+\nu_3$	s	6651.538	6651.540	−0.002
2	1	E'	$\nu_1+\nu_3$	s	6653.082	6653.098	−0.016
2	1	E''	$\nu_1+\nu_3$	s	6653.864	6653.364	0.500
2	0	E'	$\nu_1+\nu_3$	s	6656.415	6656.516	−0.101
2	0	E''	$\nu_1+\nu_3$	a	6657.122	6657.101	0.021
2	2	A_2'	$\nu_1+\nu_3$	s	6709.141	6708.980	0.161
2	2	A_2''	$\nu_1+\nu_3$	a	6709.962	6709.633	0.329
2	1	A_2''	$\nu_1+\nu_3$	a	6720.105	6720.056	0.049
2	1	E'	$\nu_1+\nu_3$	a	6720.618	6720.493	0.125
2	0	E'	$\nu_1+\nu_3$	s	6724.162	6724.185	−0.023
2	0	E''	$\nu_1+\nu_3$	a	6724.623	6724.659	−0.036
0	0	E'	$\nu_1+2\nu_4$	s	6546.987	6546.987	0.000
0	0	E''	$\nu_1+2\nu_4$	a	6548.449	6548.449	0.000
1	1	A_2'	$\nu_1+2\nu_4$	a	6559.895	6559.922	−0.027
1	0	E'	$\nu_1+2\nu_4$	s	6567.492	6567.504	−0.012
1	1	E''	$\nu_1+2\nu_4$	s	6567.904	6567.960	−0.056
1	0	E''	$\nu_1+2\nu_4$	a	6568.657	6568.730	−0.073
1	1	E'	$\nu_1+2\nu_4$	a	6569.257	6569.269	−0.012
2	2	E'	$\nu_1+2\nu_4$	s	6582.047	6582.056	−0.009
2	2	E''	$\nu_1+2\nu_4$	a	6583.439	6583.476	−0.037
2	1	A_2''	$\nu_1+2\nu_4$	s	6599.495	6599.514	−0.019
2	2	A_2'	$\nu_1+2\nu_4$	s	6601.051	6600.952	0.099
2	2	A_2''	$\nu_1+2\nu_4$	a	6602.177	6602.120	0.057
2	0	E'	$\nu_1+2\nu_4$	s	6608.463	6608.506	−0.043
2	0	E''	$\nu_1+2\nu_4$	a	6609.322	6609.348	−0.026
2	0	E''	$\nu_1+2\nu_4$	a	6609.323	6609.348	−0.025
2	1	E'	$\nu_1+2\nu_4$	a	6609.784	6609.876	−0.092
2	2	E''	$\nu_1+2\nu_4$	a	6640.194	6640.470	−0.276
2	1	E'	$\nu_3+2\nu_4$	a	6700.714	6699.362	1.352
2	2	E'	$\nu_3+2\nu_4$	s	6702.047	6703.073	−1.026
2	1	A_2'	$\nu_3+2\nu_4$	a	6713.529	6712.830	0.699

In this case our 'local' mode basis functions are used as reference and provide approximate labels for the eigenstates. The problem with this approach (as well as many other assigning approaches) is the strong mixing of basis set functions at high excitations which gives rise to the ambiguity in assignment. As a manifestation of the quality of the assignment we also provide values of the corresponding largest expansion coefficients, see the $|C_i|^2$−column in Table 7: small numbers (less than 0.5) indicate strong mixing of reference states and show that the suggested quantum numbers can be ambiguous.

Table 6
Comparison of the theoretical term values (cm^{-1}) of $^{15}NH_3$, from this work (BYTe-15) and computed by Huang et al. [47]. See Table 7 for the description of the notations.

Γ_{vib}	v_1	v_2	v_3	l_3	v_4	l_4	τ_{tor}	BYTe-15	HSL-2	BYTe-HSL
A_1'	0	0	0	0	0	0	0	0.00	0.00	0.00
A_2''	0	0	0	0	0	0	1	0.76	0.76	0.00
A_1'	0	1	0	0	0	0	0	928.46	928.47	−0.01
A_2''	0	1	0	0	0	0	1	962.89	962.93	−0.04
A_1'	0	2	0	0	0	0	0	1591.18	1591.18	0.00
A_2''	0	2	0	0	0	0	1	1870.85	1870.82	0.03
A_1'	0	3	0	0	0	0	0	2369.31	2369.33	−0.02
A_2''	0	3	0	0	0	0	1	2876.13	2876.12	0.01
A_1'	0	0	0	2	0	0	0	3210.43	3210.51	−0.08
A_2''	0	0	0	2	0	0	1	3212.12	3212.08	0.04
A_1'	1	0	0	0	0	0	0	3333.22	3333.27	−0.05
A_2''	1	0	0	0	0	0	1	3334.16	3334.25	−0.09
A_1'	0	4	0	0	0	0	0	3438.72	3438.70	0.02
A_2''	0	4	0	0	0	0	1	4034.03	4033.67	0.36
A_1'	0	1	0	2	0	0	0	4105.77	4105.95	−0.18
A_2''	0	1	0	2	0	0	1	4161.85	4161.73	0.12
A_1'	1	1	0	0	0	0	0	4288.02	4288.02	0.00
A_2''	1	1	0	0	0	0	1	4312.30	4312.29	0.01
A_1'	0	5	0	0	0	0	0	4662.71	4662.23	0.48
A_1'	0	2	0	2	0	0	0	4740.39	4743.57	−3.18
A_1'	0	0	0	3	0	3	0	4832.84	4832.55	0.29
A_2''	0	0	0	3	0	3	1	4834.25	4834.26	−0.01
A_1'	1	2	0	0	0	0	0	4995.22	4992.68	2.54
A_1'	0	0	1	1	1	1	0	5058.33	5055.98	2.35
A_2''	0	0	1	1	1	1	1	5058.75	5056.20	2.55
A_2''	0	2	0	2	0	0	1	5074.97	5076.68	−1.71
A_2''	1	2	0	0	0	0	1	5221.82	5220.15	1.67
A_2''	0	5	0	0	0	0	1	5322.90	5322.97	−0.07
A_1'	0	3	0	2	0	0	0	5579.27	5582.89	−3.62
A_1'	0	1	0	3	0	3	0	5704.65	5705.12	−0.47
A_1'	1	3	0	0	0	0	0	5723.13	5721.57	1.56
A_2''	0	1	0	3	0	3	1	5773.60	5774.00	−0.40
A_1'	0	6	0	0	0	0	0	6002.36	6001.83	0.53
A_1'	0	1	1	1	1	1	0	6004.37	6007.44	−3.07
A_2''	0	1	1	1	1	1	1	6030.73	6031.88	−1.15
A_2''	0	3	0	2	0	0	1	6106.56	6109.59	−3.03
A_2''	1	3	0	0	0	0	1	6208.93	6208.84	0.09
A_1'	0	2	0	3	0	3	0	6330.11	6333.51	−3.40
A_1'	0	0	0	4	0	0	0	6346.25	6343.14	3.11
A_2''	0	0	0	4	0	0	1	6350.08	6344.21	5.87
A_1'	2	0	0	0	0	0	0	6506.86	6512.69	−5.83
A_2''	2	0	0	0	0	0	1	6508.66	6514.29	−5.63
A_1'	1	0	0	2	0	0	0	6595.10	6597.04	−1.94
A_2''	1	0	0	2	0	0	1	6595.98	6597.93	−1.95
A_1'	1	0	0	2	0	0	0	6634.75	6637.61	−2.86
A_2''	1	0	0	2	0	0	1	6636.48	6638.79	−2.31
A_1'	0	4	0	2	0	0	0	6680.14	6682.30	−2.16
A_2''	0	2	0	3	0	3	1	6692.05	6694.31	−2.26

Recognizing the importance of the conventional 'normal' mode quantum numbers, we map our 'local' modes to the 'normal' mode quantum numbers using the same procedure as in Ref. [48]. It should be noted however that there is no direct transformation between these two labelling schemes. Furthermore due to the approximate nature of the assignment in some cases we obtain ambiguous normal mode quantum numbers, which do not always correspond to the experimental normal mode

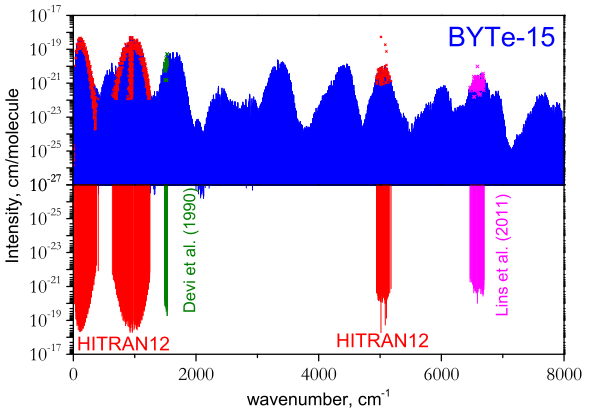

Fig. 1. Absorption of $^{15}NH_3$ at $T=296$ K (log-scale): The theoretical (BYTe-15 in the upper display) *vs.* experimental line intensities (bottom) from HITRAN 2012, by Devi et al. [39] and Lins et al. [41]. The experimental data points are repeated in the upper display as crosses for a better illustration of the agreement between theoretical and experimental intensities, where a number of outliers in the HITRAN data set is also clearly visible.

labels. Again, the value $|C_i|^2$ can be used as measure of this ambiguity.

We follow Ref. [63] and define the normal mode quantum numbers as given by

$$n_1, n_2, n_3, n_4, L_3, L_4, L, \Gamma_{\rm vib}, J, K, i, \Gamma_{\rm rot}, \Gamma_{\rm tot}, \quad (2)$$

where $L_3=|l_3|$, $L_4=|l_4|$, $L=|l|$, $K=|k|$. Here n_i, $(i=1,2,3,4)$ are the vibrational normal mode quantum numbers, l_3, l_4, and l are the vibrational angular momentum labels; J is the total angular momentum quantum number, $k=-J,\ldots,J$ is the projection of the total angular momentum on the molecule fixed axis z; $i=s/a$ is the inversion symmetry of the vibrational motion; and $\Gamma_{\rm vib}$, $\Gamma_{\rm rot}$ and $\Gamma_{\rm tot}$ are the symmetry species of the rotational, vibrational, and total internal wave-functions in the molecular symmetry group $D_{3h}(M)$, respectively, spanning A_1', A_1'', A_2', A_2'', E', and E''. As was argued by Down et al. [63], the definition of the signs of the vibrational angular momentum quantum numbers l_3, l_4 and l is ambiguous (as ambiguous the sign of k). Therefore we follow the suggestion of Down et al. [63] and use the absolute values $L_i=|l_i|=n_i, n_i-i, \ldots, 0\ (1)$ instead.

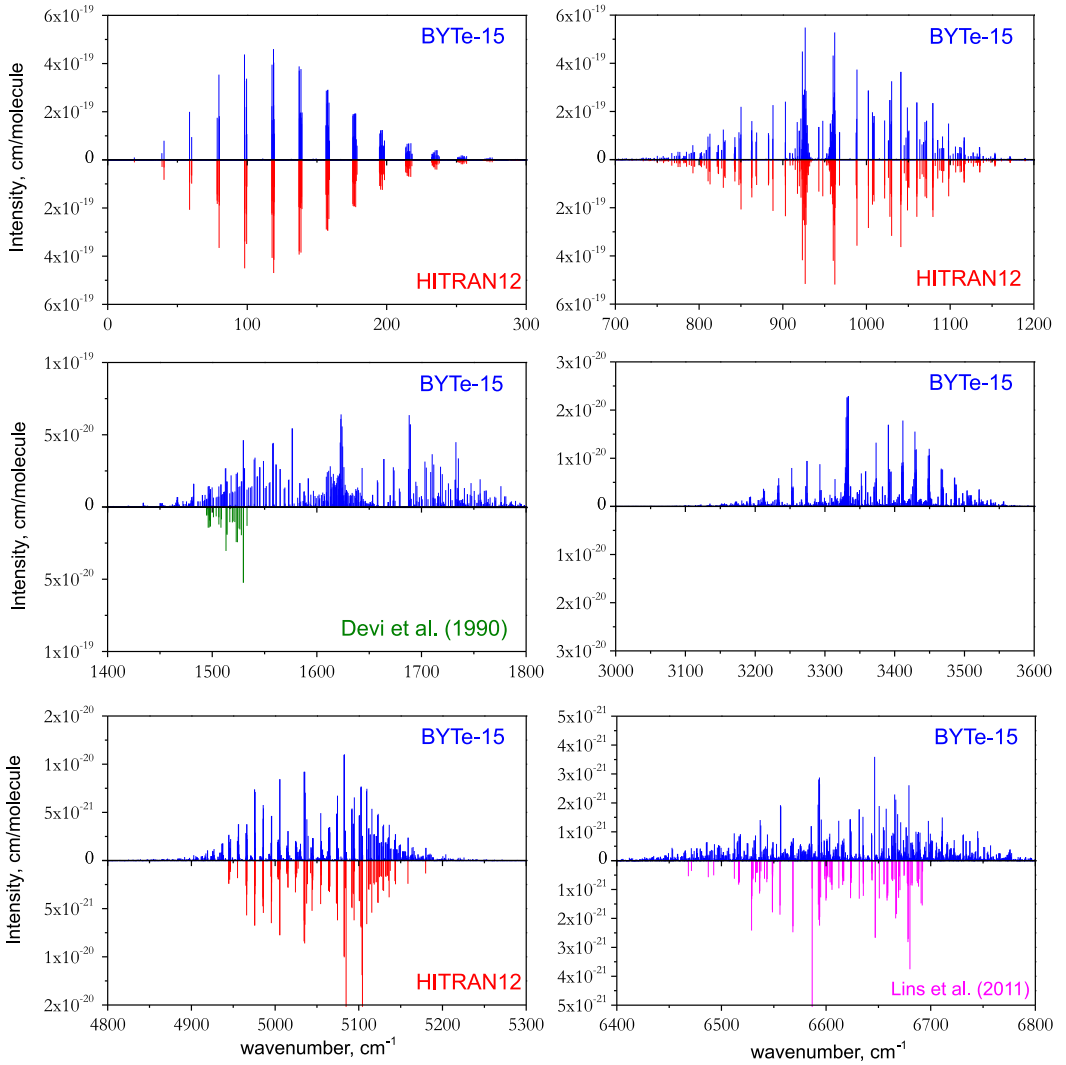

Fig. 2. Absorption of $^{15}NH_3$ at $T=296$ K: The theoretical (BYTe-15) vs. experimental line intensities (bottom) from HITRAN 2012, by Devi et al. [39] and Lins et al. [41]. The intensities of the strong 3 μm band, which is also shown, are not known experimentally.

Table 7
Extract from the energy file.

1 N	2 $\tilde{E}$	3 g_{tot}	4 J	5 Γ_{tot}	6 n_1	7 n_2	8 n_3	9 L_3	10 n_4	11 L_4	12 L	13 Γ_{vib}	14 s/a	15 J	16 K	17 Γ_{rot}	18 $\lvert C_i\rvert^2$	19 v_1	20 v_2	21 v_3	22 v_4	23 v_5	24 v_6
6997	21756.187127	8	0	5	0	0	2	0	9	9	9	5	2	0	0	1	0.03	0	1	1	0	9	1
6998	21774.591859	8	0	5	0	0	0	0	13	3	3	5	2	0	0	1	0.49	0	0	0	0	13	1
6999	21813.705372	8	0	5	0	0	4	4	5	5	9	5	2	0	0	1	0.07	1	1	2	0	5	1
7000	21827.357350	8	0	5	0	0	1	1	11	7	6	5	2	0	0	1	0.15	0	1	0	0	11	1
7001	21847.709371	8	0	5	0	0	3	3	7	3	0	5	2	0	0	1	0.02	1	2	0	0	7	1
7002	21904.095288	8	0	5	0	0	4	4	5	1	3	5	2	0	0	1	0.23	1	1	2	0	5	1
7003	21965.241710	8	0	5	0	0	1	1	11	1	0	5	2	0	0	1	0.25	0	1	0	0	11	1
7004	21995.383165	8	0	5	0	0	3	1	7	1	0	5	2	0	0	1	0.08	0	2	1	0	7	1
7005	22042.709382	8	0	5	0	0	2	0	9	3	3	5	2	0	0	1	0.04	0	1	0	0	10	3
7006	1624.202046	4	0	6	0	0	0	0	1	1	1	6	2	0	0	1	0.95	0	0	0	0	1	1
7007	2577.590496	4	0	6	0	1	0	0	1	1	1	6	2	0	0	1	0.92	0	0	0	0	1	3
7008	3235.338490	4	0	6	0	0	0	0	2	2	2	6	2	0	0	1	0.92	0	0	0	0	2	1
7009	3435.474680	4	0	6	0	0	1	1	0	0	1	6	2	0	0	1	0.57	0	1	0	0	0	1
7010	3487.312457	4	0	6	0	2	0	0	1	1	1	6	2	0	0	1	0.90	0	0	0	0	1	5
7011	4181.269381	4	0	6	0	1	0	0	2	2	2	6	2	0	0	1	0.91	0	0	0	0	2	3
7012	4421.488494	4	0	6	0	1	1	1	0	0	1	6	2	0	0	1	0.54	0	1	0	0	0	3
7013	4506.966214	4	0	6	0	3	0	0	1	1	1	6	2	0	0	1	0.87	0	0	0	0	1	7
7014	4794.204888	4	0	6	0	0	0	0	3	1	1	6	2	0	0	1	0.67	0	0	0	0	3	1
7015	4950.851210	4	0	6	1	0	0	0	1	1	1	6	2	0	0	1	0.23	0	1	0	0	1	1
7016	5041.943254	4	0	6	0	0	1	1	1	1	2	6	2	0	0	1	0.56	0	1	0	0	1	1
7017	5094.587715	4	0	6	0	2	0	0	2	2	2	6	2	0	0	1	0.89	0	0	0	0	2	5
7018	5333.136103	4	0	6	0	2	1	1	0	0	1	6	2	0	0	1	0.50	0	1	0	0	0	5
7019	5677.155784	4	0	6	0	4	0	0	1	1	1	6	2	0	0	1	0.80	0	0	0	0	1	9
7020	5741.023124	4	0	6	0	1	0	0	3	1	1	6	2	0	0	1	0.68	0	0	0	0	3	3
7021	5920.791213	4	0	6	1	1	0	0	1	1	1	6	2	0	0	1	0.24	0	1	0	0	1	3
7022	6020.013978	4	0	6	0	1	1	1	1	1	2	6	2	0	0	1	0.52	0	1	0	0	1	3
7023	6127.858605	4	0	6	0	3	0	0	2	2	2	6	2	0	0	1	0.85	0	0	0	0	2	7
7024	6302.666416	4	0	6	0	3	1	1	0	0	1	6	2	0	0	1	0.48	0	1	0	0	0	7
7025	6368.587533	4	0	6	0	0	0	0	4	2	2	6	2	0	0	1	0.44	0	0	0	0	4	1
7026	6423.454535	4	0	6	0	0	0	0	4	4	4	6	2	0	0	1	0.57	0	0	0	0	4	1
7027	6548.449000	4	0	6	1	0	0	0	2	2	2	6	2	0	0	1	0.18	0	1	0	0	2	1
7028	6597.498000	4	0	6	1	0	1	1	0	0	1	6	2	0	0	1	0.19	2	0	0	0	0	1

Column	Notation	
1	N	Level number (row)
2	$\tilde{E}$	Term value (in cm^{-1})
3	g_{tot}	Total degeneracy
4	J	Rotational quantum number
5	Γ_{tot}[a]	Total symmetry in D_{3h}(M)
6,7,8,9	n_1-n_4	Normal mode vibrational quantum numbers (see [63])
10,11	L_3, L_4	Vibrational angular momenta quantum numbers
12	L	Total vibrational angular momentum quantum number
13	Γ_{vib}[a]	Symmetry of the vibrational contribution in D_{3h}(M)
14	s/a	Inversion symmetry of the vibrational motion; (1,2) are used for (s,a), respectively
15	J	Rotational quantum number (the same as column 2)
16	K	Rotational quantum number, projection of J onto the z-axis
17	Γ_{rot}[a]	Symmetry of the rotational contribution in D_{3h}(M)
18	$\lvert C_i^2\rvert$	Largest coefficient used in the assignment
19-24	v_1-v_6	Local mode vibrational quantum numbers (see [48])

[a] The symmetry labels (1,2,3,4,5,6) are used for (A_1', A_2', E', A_1'', A_2'', E''), respectively.

The symmetries of the initial and final states are important for the line intensities, which is manifested by the selection rules and the nuclear statistical weights g_{ns}. Similar to the main isotopologue of ammonia, the ro-vibrational states with the symmetries of A_1' and A_1'' do not exist (i.e. the corresponding $g_{ns}=0$). The non-zero nuclear statistical weights factors are 8, 4, 8, 4 for A_2', E', A_2'', E'', respectively, which are different from those of $^{14}NH_3$ owning to the different nuclear spin of ^{15}N, 1 against 1/2 of ^{14}N. The TROVE approach uses the symmetrically adapted basis set, which gives the symmetry labels of the eigenstates automatically. The selection rules are the following

$$A_2' \leftrightarrow A_2'' \,, E' \leftrightarrow E'' \tag{3}$$

and

$$\Delta J = J' - J'' = 0, \pm 1, \quad J' + J'' \geq 1. \tag{4}$$

The non-existing pure vibrational ($J=0$) A_1' and A_1'' term values are also included into the line list with the total statistical weight $g_{tot}=0$, which can be useful as band centers.

Table 8
Extract from the transition file.

i'	i''	$A_{i'\leftarrow i''}/s^{-1}$
623528	445704	1.5466e−08
1737233	1846711	1.1752e−07
1334663	1430969	2.4884e−06
446023	393427	1.1053e−01
623718	688990	9.7052e−08
906264	688810	7.0643e−10
483622	426792	1.7703e−02
483793	539604	2.1314e−07
689346	623432	3.3598e−03
502670	343967	4.9180e−03
1737113	2073678	2.3521e−06
118614	148621	2.7272e−02
344060	502369	1.0103e−09
1958031	1846618	1.1248e+00
1529207	1631501	1.7843e−02
561064	623436	7.7197e−03
1919239	2034874	1.5173e−09
21841	12171	1.1518e−03

With our computed energies of $^{15}NH_3$ we obtain the partition function of 1165.4 which can be compared to the room-temperature partition function supplied by HITRAN of 1152.7 by Fischer et al. [69].

4. Conclusion

In this paper a new synthetic line list for $^{15}NH_3$ is presented. This line list should be applicable for describing absorption of this molecule for temperatures up to 300 K. The $^{15}NH_3$ line list has already proven useful for analysis of the experimental spectra by Čermák et al. [45] where it was applied for assignment of the 2.3 μm VECSEL spectra of $^{15}NH_3$.

Acknowledgments

This work is supported by ERC Advanced Investigator Project 267219. I thank J. Tennyson for helpful discussions and suggestions. I also thank P. Čermák and P. Cacciani for suggestions related to the ammonia line list.

References

[1] Abbas MM, LeClair A, Owen T, Conrath BJ, Flasar FM, Kunde VG, et al. The nitrogen isotopic ratio in Jupiter's atmosphere from observations by the Composite Infrared Spectrometer on the Cassini spacecraft. Astrophys J 2004;602:1063–74. http://dx.doi.org/10.1086/381084.

[2] Schilke P, Walmsley CM, Mauersberger R. Peculiar $^{15}NH_3$ toward NGC-7538-IRS-1. Astron Astrophys 1991;247:516–24.

[3] Charnley SB, Rodgers SD. The end of interstellar chemistry as the origin of nitrogen in comets and meteorites. Astrophys J 2002;569:L133–7. http://dx.doi.org/10.1086/340484.

[4] Lis DC, Wootten A, Gerin M, Roueff E. Nitrogen isotopic fractionation in interstellar ammonia. Astrophys J Lett 2010;710:L49–52. http://dx.doi.org/10.1088/2041-8205/710/1/L49.

[5] Gerin M, Marcelino N, Biver N, Roueff E, Coudert LH, Elkeurti M, et al. Detection of $^{15}NH_2D$ in dense cores: a new tool for measuring the $^{14}N/^{15}N$ ratio in the cold ISM. Astron Astrophys 2009;498:L9–12. http://dx.doi.org/10.1051/0004-6361/200911759.

[6] Fouchet T, Lellouch E, Bezard B, Encrenaz T, Drossart P, Feuchtgruber H, et al. ISO-SWS observations of Jupiter: Measurement of the ammonia tropospheric profile and of the $^{15}N/^{14}N$ isotopic ratio. Icarus 2000;143:223–43. http://dx.doi.org/10.1006/icar.1999.6255.

[7] Fouchet T, Irwin PGJ, Parrish P, Calcutt SB, Taylor FW, Nixon CA, et al. Search for spatial variation in the Jovian $^{15}N/^{14}N$ ratio from Cassini/CIRS observations. Icarus 2004;172:50–8. http://dx.doi.org/10.1016/j.icarus.2003.11.011.

[8] Harper LA, Sharpe RR. Atmospheric ammonia: issues on transport and nitrogen isotope measurement. Atmos Environ 1998;32:273–7. http://dx.doi.org/10.1016/S1352-2310(97)00240-9.

[9] Pizzarello S, Williams LB. Ammonia in the early solar system: an account from carbonaceous meteorites. Astrophys J 2012;749:161. http://dx.doi.org/10.1088/0004-637X/749/2/161.

[10] Mumma MJ, Charnley SB. The chemical composition of comets-emerging taxonomies and natal heritage. In: Faber SM, VanDishoeck E. editors. Annu Rev Astron Astrophys, vol. 49, 2011. p. 471–524. http://dx.doi.org/10.1146/annurev-astro-081309-130811.

[11] Fletcher LN, Greathouse T, Orton G, Irwin P, Mousis O, Sinclair J, et al. The origin of nitrogen on Jupiter and Saturn from the $^{15}N/^{14}N$ ratio. Icarus 2014;238:170–90. http://dx.doi.org/10.1016/j.icarus.2014.05.007 ⟨http://www.sciencedirect.com/science/article/pii/S0019103514002516⟩.

[12] Shimzu FO, Shimizu T. Infrared spectrum of 10 μm band of $^{15}NH_3$. J Mol Spectrosc 1970;36:94–109. http://dx.doi.org/10.1016/0022-2852(70)90127-X.

[13] Carlotti M, Trombetti A, Velino B, Vrbancich J. The rotation-inversion spectrum of $^{15}NH_3$. J Mol Spectrosc 1980;83:401–7. http://dx.doi.org/10.1016/0022-2852(80)90064-8.

[14] Sasada H. Microwave inversion spectrum of $^{15}NH_3$. J Mol Spectrosc 1980;83:15–20. http://dx.doi.org/10.1016/0022-2852(80)90307-0.

[15] Fusina L, Carlotti M, Dilonardo G, Murzin SN, Stepanov ON. Pure inversion and inversion-totation spectra of $^{15}ND_3$ in the ground-state. J Mol Spectrosc 1991;147:71–83. http://dx.doi.org/10.1016/0022-2852(91)90169-B.

[16] Schatz W, Renk KF, Fusina L, Izatt JR. Far-infrared laser-emission spectroscopy on ammonia isotopomers. Appl Phys B—Lasers Opt 1994;59:453–65. http://dx.doi.org/10.1007/BF01081068.

[17] Urban S, Klee S, Yamada KMT. Ground-state ro-inversional transitions of $^{15}NH_3$ in the far-infrared region. J Mol Spectrosc 1994;168:384–9. http://dx.doi.org/10.1006/jmsp.1994.1287.

[18] Cohen EA. ν_4 state inversion spectra of $^{15}NH_3$ and $^{14}NH_3$. J Mol Spectrosc 1980;79:496–501. http://dx.doi.org/10.1016/0022-2852(80)90227-1.

[19] Job VA, Patel ND, D'Cunha R, Kartha VB. High-resolution diode-laser measurements on the ν_2 bands of $^{14}NH_3$ and $^{15}NH_3$. J Mol Spectrosc 1983;101:48–60. http://dx.doi.org/10.1016/0022-2852(83)90005-X.

[20] Urban S, Papoušek D, Belov SP, Krupnov AF, Tretyakov MY, Yamada K, et al. A simultaneous analysis of the microwave, submillimeter-wave, and infrared transitions between the ground and ν_2 inversion-rotation levels of $^{15}NH_3$. J Mol Spectrosc 1983;101:16–29. http://dx.doi.org/10.1016/0022-2852(83)90003-6.

[21] Urban S, D'Cunha R, Rao KN. Identification of forbidden vibration-rotation transitions in $^{15}NH_3$. J Mol Spectrosc 1984;106:64–71. http://dx.doi.org/10.1016/0022-2852(84)90083-3.

[22] Urban S, D'Cunha R, Rao KN, Papoušek D. The $\Delta K = \pm 2$ perturbation-allowed ν_4 band and inversion rotation energy-levels of $^{15}NH_3$. J Mol Spectrosc 1985;111:361–76. http://dx.doi.org/10.1016/0022-2852(85)90012-8.

[23] D'Cunha R, Urban S, Rao KN, Henry L, Valentin A. The ν_2 band of $^{15}NH_3$. J Mol Spectrosc 1985;111:352–60. http://dx.doi.org/10.1016/0022-2852(85)90011-6.

[24] Iwahori J, Ueda Y, Nakagawa K. Laser stark spectroscopy of the ν_2 fundamental band of $^{15}NH_3$. J Mol Spectrosc 1986;117:1–14, http://dx.doi.org/10.1016/0022-2852(86)90087-1.

[25] Urban S, D'Cunha R, Manheim J, Rao KN. High-J transitions in the ν_2 bands of $^{14}NH_3$ and $^{15}NH_3$. J Mol Spectrosc 1986;118:298–309.

[26] Anders S, Jonuscheit J, Lehner U, Sarka K, Schrotter HW. High-resolution coherent anti-Stokes Raman spectra of the Q-branches of the ν_1 bands of $^{14}NH_3$ and $^{15}NH_3$ and their assignment. J Raman Spectrosc 2000;31:711–8 http://dx.doi.org/10.1002/1097-4555(200008/09)31:8/9 711::AID-JRS599 3.0.CO;2-X.

[27] Fusina L, Nivellini G, Spezzano S. The ν_1 and ν_3 band system of $^{15}NH_3$. Mol Phys 2011;109:2209–17. http://dx.doi.org/10.1080/00268976.2011.609140.

[28] Dilonardo G, Fusina L, Trombetti A, Mills IM. The υ_2, $2\upsilon_2$, $3\upsilon_2$, υ_4, and $\upsilon_2 + \upsilon_4$ bands of $^{15}NH_3$. J Mol Spectrosc 1982;92:298–325. http://dx.doi.org/10.1016/0022-2852(82)90105-9.

[29] Sasada H, Hasegawa Y, Amano T, Shimizu T. High-resolution infrared and microwave spectroscopy of the ν_4 band and $2\nu_2$ band of $^{14}NH_3$

and $^{15}NH_3$. J Mol Spectrosc 1982;96:106–30. http://dx.doi.org/10.1016/0022-2852(82)90218-1.
[30] Fusina L, Baldacchini G. The spectroscopic parameters of the $\upsilon_2=2a$ state for $^{14}NH_3$ and $^{15}NH_3$. J Mol Spectrosc 1990;141:23–8. http://dx.doi.org/10.1016/0022-2852(90)90274-T.
[31] Moriwaki Y, Nakagawa K, Shimizu T. Observation and analysis of the $\Delta\upsilon=5$ stretch overtone band transition of $^{15}NH_3$. Jpn J Appl Phys Part 1—Regul Pap Short Notes Rev Pap 1991;30:2901–7. http://dx.doi.org/10.1143/JJAP.30.2901.
[32] Lees RM, Li L, Liu Z, Xu L-H. External cavity tunable diode laser spectrum of the $\nu_1+\nu_3$ N–H stretching combination band of $^{15}NH_3$. J Mol Struct (THEOCHEM) 2006;795:134–42. http://dx.doi.org/10.1016/j.molstruc.2006.02.018.
[33] Lees RM, Li L, Xu L-H. New VISTA on ammonia in the 1.5 μm region: Assignments for the $\nu_3+2\nu_4$ bands of $^{14}NH_3$ and $^{15}NH_3$ by isotopic shift labeling. J Mol Spectrosc 2008;251:241–51. http://dx.doi.org/10.1016/j.jms.2008.03.013.
[34] Karyakin EN, Krupnov AF, Papoušek D, Shchurin JM, Urban S. Submillimeter-wave rotation-inversion transition $J=1-0$, $\Delta K=0$ of $^{14}NH_3$ and $^{15}NH_3$ in ν_2 state. J Mol Spectrosc 1977;66:171–3. http://dx.doi.org/10.1016/0022-2852(77)90332-0.
[35] Urban S, Misra P, Rao KN. The $\nu_1+\nu_2$ and $\nu_1+\nu_2-\nu_2$ bands of $^{14}NH_3$ and $^{15}NH_3$. J Mol Spectrosc 1985;114:377–94. http://dx.doi.org/10.1016/0022-2852(85)90233-4.
[36] Sasada H, Schwendeman RH. High-resolution spectroscopy of the $\upsilon_2=2a\leftarrow s$ $\upsilon_2=1$ s band of $^{15}NH_3$. J Mol Spectrosc 1986;117:331–41. http://dx.doi.org/10.1016/0022-2852(86)90158-X.
[37] D'Cunha R. The a 2 $\upsilon_2\leftarrow s$ υ_2 bands $^{14}NH_3$ and $^{15}NH_3$. J Mol Spectrosc 1987;122:130–4. http://dx.doi.org/10.1016/0022-2852(87)90223-2.
[38] Varanasi P, Wyant P. Intensities and line-shapes in the ν_2-fundamentals of $^{14}NH_3$ and $^{15}NH_3$. J Quant Spectrosc Radiat Transf 1981;25:311–7. http://dx.doi.org/10.1016/0022-4073(81)90080-7.
[39] Devi VM, Rao KN, Pracna P, Urban S. Intensities in the ν_4 band of $^{15}NH_3$. J Mol Spectrosc 1990;143:18–24.
[40] Siemsen KJ, Madej AA, Whitford BG. Absolute frequency measurement of the $sp(8,6)$ transition of $^{15}NH_3$. J Mol Spectrosc 1995;174:613–4. http://dx.doi.org/10.1006/jmsp.1995.0030.
[41] Lins B, Pflaum F, Engelbrecht R, Schmauss B. Absorption line strengths of $^{15}NH_3$ in the near infrared spectral region. Appl Phys B—Lasers Opt 2011;102:293–301. http://dx.doi.org/10.1007/s00340-010-4217-1.
[42] Rothman LS, Gordon IE, Babikov Y, Barbe A, Benner DC, Bernath PF, et al. The *HITRAN*2012 molecular spectroscopic database. J Quant Spectrosc Radiat Transf 2013;130:4–50. http://dx.doi.org/10.1016/jqsrt.2013.07.002.
[43] Orr BJ, Oka T. Determination of electric-dipole moment for ν_2 vibrational-state of $^{15}NH_3$ by infrared-infrared double resonances. J Mol Spectrosc 1977;66:302–13. http://dx.doi.org/10.1016/0022-2852(77)90219-3.
[44] Dilonardo G, Trombetti A, Velino B. Dipole-moment for the $\upsilon_2=1$ vibrational-state of $^{15}NH_3$ by saturation laser Stark spectroscopy. Chem Phys Lett 1981;80:352–4. http://dx.doi.org/10.1016/0009-2614(81)80124-8.
[45] Čermák P, Hovorka J, Veis P, Cacciani P, Cosléou J, Romh JE, et al. Spectroscopy of $^{14}NH_3$ and $^{15}NH_3$ in the 2.3 μm spectral range with a new VECSEL laser source. J Quant Spectrosc Radiat Transf 2014;137:13–22. http://dx.doi.org/10.1016/j.jqsrt.2014.01.005 URL: ⟨http://www.sciencedirect.com/science/article/pii/S0022407314000089⟩.
[46] Földes T, Golebiowski D, Herman M, Softley T, Di Lonardo G, Fusina L. Low-temperature high-resolution absorption spectrum of $^{14}NH_3$ in the $\nu_1+\nu_3$ band region (1.51 μm). Mol Phys 2014;112:2407–18. http://dx.doi.org/10.1080/00268976.2014.904944.
[47] Huang X, Schwenke DW, Lee TJ. Rovibrational spectra of ammonia. II. Detailed analysis, comparison, and prediction of spectroscopic assignments for $^{14}NH_3$, $^{15}NH_3$, and $^{14}ND_3$. J Chem Phys 2011;134:044321. http://dx.doi.org/10.1063/1.3541352.
[48] Yurchenko SN, Barber RJ, Tennyson J. A variationally computed line list for hot NH_3. Mon Not R Astron Soc 2011;413:1828–34. http://dx.doi.org/10.1111/j.1365-2966.2011.18261.x.
[49] Yurchenko SN, Thiel W, Jensen P. Theoretical ROVibrational Energies (TROVE): A robust numerical approach to the calculation of rovibrational energies for polyatomic molecules. J Mol Spectrosc 2007;245:126–40. http://dx.doi.org/10.1016/j.jms.2007.07.009.
[50] Beaulieu JP, Tinetti G, Kipping DM, Ribas I, Barber RJ, Cho JYK, et al. Methane in the atmosphere of the transiting hot Neptune GJ 436b? Astrophys J 2011;731:16. http://dx.doi.org/10.1088/0004-637X/731/1/16.
[51] Lucas PW, Tinney CG, Burningham B, Leggett SK, Pinfield DJ, Smart R, et al. The discovery of a very cool, very nearby brown dwarf in the Galactic plane. Mon Not R Astron Soc 2010;408:L56–60, http://dx.doi.org/10.1111/j.1745-3933.2010.00927.x.
[52] Yurchenko SN, Barber RJ, Tennyson J, Thiel W, Jensen P. Towards efficient refinement of molecular potential energy surfaces: ammonia as a case study. J Mol Spectrosc 2011;268:123–9, http://dx.doi.org/10.1016/j.jms.2011.04.005.
[53] Yurchenko SN, Barber RJ, Yachmenev A, Thiel W, Jensen P, Tennyson J. A variationally computed $T=300$ K line list for NH_3. J Phys Chem A 2009;113:11845–55. http://dx.doi.org/10.1021/jp9029425.
[54] Yachmenev A, Yurchenko SN, Paidarova I, Jensen P, Thiel W, Sauer SPA. Thermal averaging of the indirect nuclear spin-spin coupling constants of ammonia: The importance of the large amplitude inversion mode. J Chem Phys 2010;132:114305. http://dx.doi.org/10.1063/1.3359850.
[55] Sousa-Silva C, Hesketh N, Yurchenko SN, Hill C, Tennyson J. High Temperature partition functions and thermodynamic data for ammonia and phosphine. J Quant Spectrosc Radiat Transf 2014;142:66–74. http://dx.doi.org/10.1016/j.jqsrt2014.03.012.
[56] Noumeroff B. Méthode nouvelle de la determination des orbites et le calcul des éphémérides en tenant compte des perturbations, vol. 2, Moscow, Gosudarsvennoe Izdatel'stvo; 1923. p. 188–259.
[57] Cooley JW. An improved eigenvalue corrector formula for solving the Schrödinger equation for central fields. Math Comput 1961;15:363–74. http://dx.doi.org/10.1090/S0025-5718-1961-0129566-X.
[58] Yurchenko SN, Carvajal M, Jensen P, Lin H, Zheng JJ, Thiel W. Rotation-vibration motion of pyramidal XY3 molecules described in the Eckart frame: Theory and application to NH_3. Mol Phys 2005;103:359–78. http://dx.doi.org/10.1080/00268970512331517255.
[59] Shojachaghervand P, Schwendeman RH. Infrared microwave 2-photon spectroscopy of the ν_2 band of $^{15}NH_3$. J Mol Spectrosc 1983;97:306–15. http://dx.doi.org/10.1016/0022-2852(83)90269-2.
[60] Li L, Lees RM, Xu L-H. External cavity tunable diode laser spectra of the $\nu_1+2\nu_4$ stretch-bend combination bands of $^{14}NH_3$ and $^{15}NH_3$. J Mol Spectrosc 2007;243:219–26. http://dx.doi.org/10.1016/j.jms.2007.04.003.
[61] Yurchenko SN, Carvajal M, Lin H, Zheng JJ, Thiel W, Jensen P. Dipole moment and rovibrational intensities in the electronic ground state of NH_3: Bridging the gap between ab initio theory and spectroscopic experiment. J Chem Phys 2005;122:104317. http://dx.doi.org/10.1063/1.1862620.
[62] Yurchenko SN, Thiel W, Carvajal M, Lin H, Jensen P. Rotation–vibration motion of pyramidal XY_3 molecules described in the Eckart frame: The calculation of intensities with application to NH_3. Adv Quant Chem 2005;48:209–38. http://dx.doi.org/10.1016/S0065-3276(05)48014-4.
[63] Down MJ, Hill C, Yurchenko SN, Tennyson J, Brown LR, Kleiner I. Re-analysis of ammonia spectra: Updating the HITRAN $^{14}NH_3$ database. J Quant Spectrosc Radiat Transf 2013;130:260–72. http://dx.doi.org/10.1016/j.jqsrt.2013.05.027.
[64] Barber RJ, Tennyson J, Harris GJ, Tolchenov RN. A high accuracy computed water line list. Mon Not R Astron Soc 2006;368:1087–94.
[65] Tennyson J, Hill C, Yurchenko SN. Data structures for ExoMol: molecular line lists for exoplanet and other atmospheres. In: Gillaspy J, Wiese W, Podpaly Y, editors. Eighth international conference on atomic and molecular data and their applications: ICAMDATA-8, volume 1545 of AIP Conference Proceedings, 2013, pp. 186–195. http://dx.doi.org/10.1063/1.4815853.
[66] Tennyson J, Yurchenko SN. ExoMol: molecular line lists for exoplanet and other atmospheres. Mon Not R Astron Soc 2012;425:21–33. http://dx.doi.org/10.1111/j.1365-2966.2012.21440.x.
[67] Hill C, Yurchenko SN, Tennyson J. Temperature-dependent molecular absorption cross sections for exoplanets and other atmospheres. Icarus 2013;226:1673–7. http://dx.doi.org/10.1016/j.icarus.2012.07.028.
[68] Bunker PR, Jensen P. Molecular symmetry and spectroscopy. 2nd ed. Ottawa: NRC Research Press; 1998.
[69] Fischer J, Gamache RR, Goldman A, Rothman LS, Perrin A. Total internal partition sums for molecular species in the 2000 edition of the HITRAN database. J Quant Spectrosc Radiat Transf 2003;82:401–12.